catalysts

MDPI

Article

Biotemplated Mesoporous TiO_2/SiO_2 Composite Derived from Aquatic Plant Leaves for Efficient Dye Degradation

Zhiying Yan, Jiao He, Lei Guo, Yueting Li, Deliang Duan, Yongjuan Chen, Junjie Li, Fagui Yuan and Jiaqiang Wang *

Yunnan Provincial Collaborative Innovation Center of Green Chemistry for Lignite Energy, Yunnan Province Engineering Research Center of Photocatalytic Treatment of Industrial Wastewater, The Universities' Center for Photocatalytic Treatment of Pollutants in Yunnan Province, School of Chemical Sciences & Technology, School of Energy, Yunnan University, Kunming 650091, China; zhyyan@ynu.edu.cn (Z.Y.); hejiao@ynu.edu.cn (J.H.); guolei28@yeah.net (L.G.); li_yueting@126.com (Y.L.); dlduan@ynu.edu.cn (D.D.); chenyongjuan@ynu.edu.cn (Y.C.); JunJieLi@ynu.edu.cn (J.L.); yfg1221@163.com (F.Y.)

* Correspondence: jqwang@ynu.edu.cn; Tel.: +86-871-6503-1567

Academic Editors: Shaobin Wang and Xiaoguang Duan

Received: 10 January 2017; Accepted: 7 March 2017; Published: date

Abstract: The biotemplating technique is an environmental-protective high-efficiency new technology by which the resulting TiO_2 may simultaneously attain the duplication of structure and self-doping elements from biotemplate materials, which is highly desirable for photocatalytic applications. In this paper, aquatic plant leaves—including reed, water hyacinth, and duckweed—were used as both templates and silicon precursors to successfully synthesize biomorphic TiO_2/SiO_2 composite with mesoporous structures. X-ray diffraction, scanning electron microscopy, transmission electron microscopy, N_2 adsorption–desorption, and UV–visible diffuse reflectance spectra were applied to characterize the microstructures of the samples. The results show that all TiO_2/SiO_2 composites are mainly composed of an anatase phase with mesoporous structure and possess high specific surface area. Compared with commercial Degussa P25 TiO_2, all TiO_2/SiO_2 samples display intensive light-harvesting efficiency, particularly in the visible light range. The activities were evaluated by using gentian violet as a target for photocatalytic degradation experiments under simulated solar irradiation. The TiO_2/SiO_2 samples templated by reed and water hyacinth leaves exhibit high activity, while the TiO_2/SiO_2 samples obtained from duckweed are inferior to P25 in the degradation of gentian violet. A synergistic effect of SiO_2 incorporation and structural construction through biotemplating is proposed to be beneficial to photocatalytic activity.

Keywords: titanium silicon oxides; biotemplates; aquatic plants; photocatalysis

1. Introduction

Photocatalytic processes to degrade organic pollutants in water by utilizing a catalyst under solar light illumination have been proven to be potentially advantageous and useful when we have to resolve increasingly serious environmental problems [1]. As a typical environmentally benign photocatalyst, titanium dioxide (TiO_2) shows potential applications in the future because of its stability as well as the low cost. Unfortunately, the pure form of TiO_2 can only absorb a small fraction of solar energy, and currently used TiO_2 photocatalysts, such as commercial Degussa P25, exhibit low specific surface area and poor adsorption, which restrict its practical applications. To date, numerous studies have been carried out for improving the photocatalytic performance of TiO_2 through both structural modification and compositional change. One way is to prepare TiO_2 in the

form of a porous structure by applying various chemicals like supramolecular compounds or self-assembled polymers as templates [2]. Another is to dope TiO_2 with nonmetal elements (nitrogen, sulfur, carbon, etc.) [3,4], or synthesize a mixed oxide, like TiO_2/SiO_2, by utilizing an in situ technique or post treatment [5–8]. Despite great progress being made, the application of chemical templates is uneconomical and, in turn, further increases environmental pollution. Also, the introduction of additional precursor to dope elements in photocatalysts is complex and cumbersome. More important, most studies were devoted to only one of the methods, rather than both of them, and neither of the methods by which TiO_2 photocatalysts are prepared are widely applied—although the environmental problem is more and more serious—which to some extent is owing to the poor light absorption and small specific surface area of TiO_2 [3]. Therefore, it is highly desirable to develop a simple, low-cost, and environmentally friendly method to prepare efficient TiO_2 photocatalysts by concurrently modifying the structure and composition.

Nowadays, the biotemplating technique, which combines biological resources with a sol–gel synthetic method, has been widely used in templated synthesis of TiO_2, especially when inheritance of the structure/morphology from template to product is desired. The biotemplate materials are more economical and environmentally benign, which are incomparable with traditional chemical template methods. So, the biotemplating technique has attracted more and more attention. So far, many plant tissues are used as novel biotemplates for the development of promising photocatalysts. On the one hand, the hierarchical pore structures of plant tissues, which are designed favorably for photosynthesis, endow them with unique properties, particularly great light-adsorbing capability. For example, the spotlight effect of epidermal cells in leaves and the light-scattering of plant tissues would contribute to promoting light adsorption at the interior of the leaf [9,10]. When these plant tissues are pretreated with a glutaraldehyde, HCl, and $TiCl_3$ solution, their morphology and structural features can be well copied to the resulting TiO_2 via a sol–gel process [10,11]. On the other hand, plant tissues are rich in a variety of nonmetallic elements (C, N and Si etc.), which can be applied as bioprecursors for the synthesis of nonmetal-doped photocatalysts [10]. Thus, the resulting TiO_2 synthesized by employing single plant tissues as templates may simultaneously have copied the template structure and incorporated the element, which is highly desirable for photocatalytic applications. For example, Zhang et al. [11] prepared the morph-structured TiO_2 with self-doped N simultaneously by employing green leaf, which has N-rich chlorophylls, as biotemplates. The absorbance intensity of morph-TiO_2 in the visible range increases by 103%–258% compared to that of TiO_2 without a template. In addition, among the doped nonmetallic elements, silica as a dopant is typically used in TiO_2 for photocatalysis. For example, Dorian et al. [12] and Kibombo et al. [13] reported, respectively, that the introduction of SiO_2 could improve not only the specific surface area of TiO_2 photocatalysts, but also its photocatalytic performance in purifying water applications; this result was due to the improved charge carrier separation at TiO_2–SiO_2 interfaces. Also, Yang et al. [14] and Ma et al. [15] utilized rice husk and corn plant as biotemplates, respectively, to synthesize hierarchical porous TiO_2/SiO_2 composites. They found enhancement not only in the visible-light harvesting ability of TiO_2/SiO_2, but also the photocatalytic activity in the degradation of dye. Recently, Liu et al. [16] constructed hierarchical artificial leaves (TiO_2–SiO_2 photocatalyst) by using aquatic plant leaves (*Vallisneria*). The obtained TiO_2–SiO_2 replicas degraded dye 3 times better than commercial Degussa P25 TiO_2 under UV irradiation. Moreover, during the preparation process, a mesoporous directing agent as a second template and SiO_2 as a mesoporous stabilizer were simultaneously introduced. As known, the aquatic plant leaves are generally thin, soft, and even transparent, which is beneficial to allow access to the light. So far, to our knowledge, the synthesis of TiO_2/SiO_2 photocatalysts based on a single aquatic plant has not yet been reported until now.

In this work, three typical aquatic plant leaves—including reed (*Phragmites australis*), water hyacinth (*Eichhornia crassipes*), and duckweed (*Lemna minor* L.)—were adopted as both biotemplates and sources of silica to fabricate biomorphic mesoporous TiO_2/SiO_2 photocatalysts. All TiO_2/SiO_2 samples exhibit improved light-harvesting abilities and their specific surface area is higher than P25 TiO_2. The photocatalytic activities were evaluated by using gentian violet as the target for

photocatalytic degradation experiments under simulated sunlight irradiation. The results indicate that TiO_2/SiO_2 samples templated by reed and water hyacinth leaves exhibit high activity, while TiO_2/SiO_2 samples obtained from duckweed is inferior to P25 in the degradation of gentian violet. A synergistic effect on their photocatalytic activity is proposed.

2. Results and Discussion

2.1. Components, Structures, and Morphologies of TiO_2/SiO_2 Photocatalysts

The elemental components and content of the samples, estimated by X-ray fluorescence (XRF) measurement, are shown in Table 1. Aside from Ti and O existing in these samples, 15.66%, 4.22%, and 0.65% of Si was also found in reed (R-TiO_2/SiO_2), water hyacinth (WH-TiO_2/SiO_2), and duckweed (D-TiO_2/SiO_2) samples, respectively. This suggests that SiO_2 in templates was preserved after calcination. Moreover, 3.98% of C was detected in D-TiO_2/SiO_2, which could be attributed to the residual duckweed biotemplate after calcination at 450 °C.

Table 1. Elemental content and structural characteristics of the samples.

Samples	Ti [a] (%)	O [a] (%)	C [a] (%)	Si [a] (%)	d_{XRD} [b] (nm)	S_{BET} [c] ($m^2 \cdot g^{-1}$)
R-TiO_2/SiO_2	27.14	57.20	-	15.66	4.2	235
WH-TiO_2/SiO_2	45.26	50.52	-	4.22	7.7	127
D-TiO_2/SiO_2	44.84	50.53	3.98	0.65	3.5	139

[a] Elemental content estimated by X-ray fluorescence (XRF); [b] Grain size calculated by using the Scherrer equation; [c] Specific surface area obtained by using the Brunauer–Emmett–Teller (BET) model. R-TiO_2/SiO_2: reed, WH-TiO_2/SiO_2: water hyacinth, D-TiO_2/SiO_2: duckweed.

The wide-angle XRD patterns of the samples are shown in Figure 1. The diffraction peaks of the 2θ values 25.3°, 37.9°, 48.0°, 53.8°, 55.0°, 62.8°, 68.6°, 70.4°, and 75.1° correspond to (101), (004), (200), (105), (211), (116), (204), (220), and (215) crystalline phases of anatase (JCPDS card No. 84-1285), respectively. It is seen that all TiO_2/SiO_2 composites are mainly made of the anatase phase after calcination at 723 K for 6 h, except a weak peak at 30.8° corresponding to the crystalline phase of brookite in WH-TiO_2/SiO_2. There are no diffraction peaks of silica or silicates in the XRD patterns, which indicates that the silica structure in the TiO_2/SiO_2 composite, just as in the original plant leaves, is still amorphous. It has been reported that SiO_2 particles in TiO_2 grain boundaries are able to inhibit the formation of rutile by restricting the atomic rearrangement during the phase transformation [12,13,17]. Thus, the enhanced stability of the anatase phase could be due to the introduction of SiO_2. In addition, the stronger (101) diffraction peaks for R-TiO_2/SiO_2 and WH-TiO_2/SiO_2 indicated that they possessed a higher crystallinity than D-TiO_2/SiO_2. The average grain sizes of the TiO_2/SiO_2 samples, calculated by using the Scherrer equation according to (101) diffraction, are 7.7 nm for WH-TiO_2/SiO_2, 4.2 nm for R-TiO_2/SiO_2, and 3.5 nm for D-TiO_2/SiO_2 (Table 1).

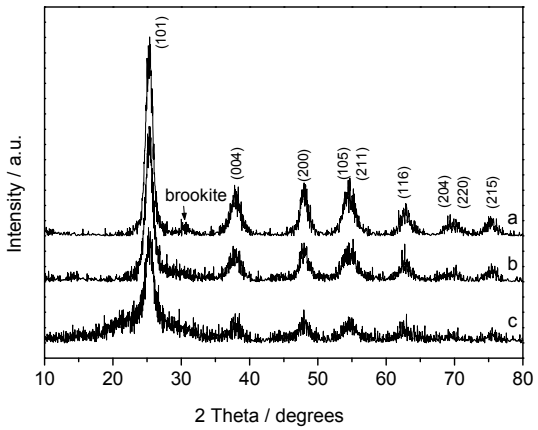

Figure 1. XRD patterns of (a) WH-TiO_2/SiO_2; (b) R-TiO_2/SiO_2; and (c) D-TiO_2/SiO_2.

The Fourier-transform infrared (FTIR) spectra of the biotemplated TiO_2/SiO_2 samples are shown in Figure 2. A typical Ti–O–Ti stretching vibration in the range of 500–590 cm^{-1} corresponds to the anatase phase. The absorption peaks at about 1630 and 3430 cm^{-1} are attributed to the bending and stretching vibrations of surface water molecules. Finally, the bands at 470, 800, and 1096 cm^{-1} are associated with the Si–O–Si deformation pattern, and symmetric and asymmetric stretching vibration, respectively [13,18]. These bands are stronger in the R-TiO_2/SiO_2 sample than in the other two, indicating that the Si present in the aquatic plant leaves was introduced to the resulting TiO_2/SiO_2 composites. In particular, a very weak band at 952 cm^{-1} due to Ti–O–Si linkage could be found in the R-TiO_2/SiO_2 sample, further suggesting that the SiO_2 was bonded to the TiO_2 particles [13,19,20]. The peak intensity of Ti–O–Si and Si–O–Si becomes less pronounced in WH-TiO_2/SiO_2 and D-TiO_2/SiO_2, probably because the low level of SiO_2 is difficult to detect using FTIR.

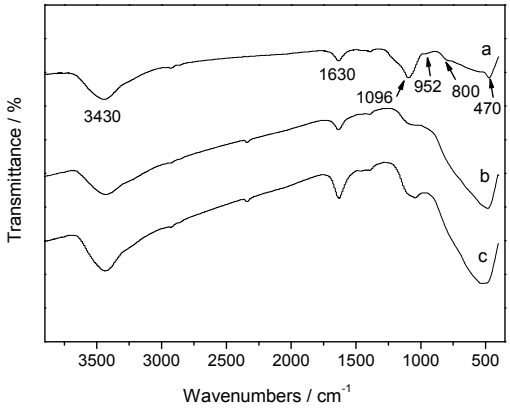

Figure 2. Fourier-transform infrared (FTIR) spectra of (a) R-TiO_2/SiO_2; (b) WH-TiO_2/SiO_2; and (c) D-TiO_2/SiO_2.

The N_2 adsorption/desorption isotherms and the pore size distribution of the R-TiO_2/SiO_2 sample derived from reed leaves are shown in Figure 3. It can be seen in Figure 3a that the N_2 sorption isotherms show a type-IV hysteresis loop in the P/P_0 range from 0.40 to 1.0, a characteristic of titania-type mesoporous materials [21]. Moreover, the hysteresis loops of type H3 suggest that the mesopores may be pile-up pores resulting from particle aggregation [22]. This result is further proved by the corresponding Barrett–Joyner–Halenda (BJH) pore size distribution shown in Figure 3b, in which the distribution range of primary pore size is from 3.5 to 30 nm. Similar mesoporous structures were obtained from the WH-TiO_2/SiO_2 and D-TiO_2/SiO_2 samples and are shown in Figure S1 (Supplementary Materials). The corresponding pore size distribution is between 5.9 and 30 nm for WH-TiO_2/SiO_2 samples, and between 6.5 and 30 nm for D-TiO_2/SiO_2 samples. The wide pore size distribution is due to the natural hierarchical structures of the plant templates [15].

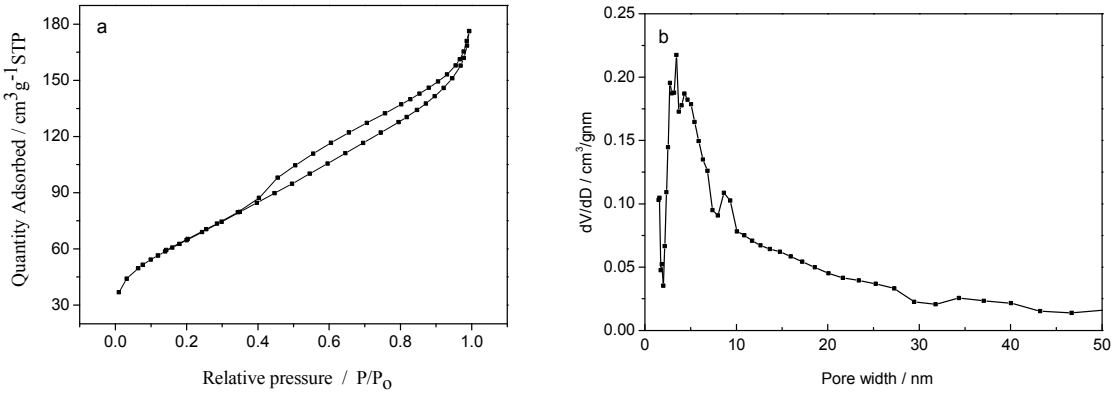

Figure 3. (**a**) Nitrogen adsorption–desorption isotherms and (**b**) Barrett–Joyner–Halenda (BJH) pore size distribution of R-TiO_2/SiO_2 samples.

As shown in Table 1, the Brunauer–Emmett–Teller (BET) specific surface areas of the TiO_2/SiO_2 samples are 235, 127, and 139 m^2/g, corresponding to the R-TiO_2/SiO_2, WH-TiO_2/SiO_2, D-TiO_2/SiO_2 samples, respectively. Particularly, the R-TiO_2/SiO_2 sample is four times more than P25 (50 $m^2 \cdot g^{-1}$) for specific surface area. As known, the biomorphic mesoporous structure is believed to improve the specific surface area of TiO_2. Besides, it is frequently reported that the introduction of SiO_2 is also capable of increasing the specific surface area of TiO_2 photocatalysts [12,13]. As a result, TiO_2/SiO_2 photocatalysts could provide more adsorption and active sites, and quicken the diffusion and transition of reactants in the photocatalytic process, ultimately benefiting the increase of photocatalytic efficiency [6,7].

Reed, water hyacinth, and duckweed are characteristic of aquatic environments. Figure 4 displays the leaf epidermal micromorphology of the three species, the hierarchical structures of the TiO_2/SiO_2 composite, and the corresponding spectra of electron diffraction from a selected area. It can be seen in Figure 4a that the original reed leaves have a linearly arrayed skeleton of veins, and vascular bundles with narrow space display a regular location pattern. In particular, many stomata at the same level of epidermal cells are regularly arranged on leaf epiderm. It is worth noting that located between the veins are convexly shaped epidermal cells, which are able to focus light like a lens within the leaf by refraction [23,24]. The original water hyacinth leaf and the original duckweed leaf, by contrast, display an irregular skeleton of veins. As seen in Figure 4c, water hyacinth leaf has an interlaced network structure formed by corrugated epidermal cells. The original duckweed leaf in Figure 4e has a disorderly venation, and epidermal cell anticlinal walls are wavy and curved. The morphologies of the prepared TiO_2/SiO_2 samples derived from original aquatic plant leaves are revealed in Figure 4b,d,f. It can be seen that the TiO_2/SiO_2 samples are similar to the epidermal microstructures of the original plant leaves, indicating that the morphologies of plant templates were inherited by samples through the biotemplating process. In particular, the Scanning electron microscopy (SEM) image of the white circle in Figure 4b displays clear papillae, just like in the reed leaf. In Figure 4d, the stomas could be observed as indicated by the arrows. It has been reported that the papillae and stomata in plants are helpful for the capture of light. So, it is desirable that TiO_2/SiO_2 samples replicate the papillae and stomata from plants, therby improving the ability to catch light and providing more adsorption and active sites in the photocatalytic process [23,24]. The energy dispersive X-ray spectroscopy (EDS) analyses shown in Figure 4g–i suggest the presence of Ti, Si, and O in the TiO_2/SiO_2 composite. Particularly, the R-TiO_2/SiO_2 sample contains more Si content than the others. This is in agreement with the result of XRF. The peaks associated with C in Figure 4g,h should be contributed to the conductive tape used in EDS experiments, while that in Figure 4i is more likely due to the sample itself. In addition, P was detected in all samples, and should be due to the residual phosphorus compounds from biotemplates.

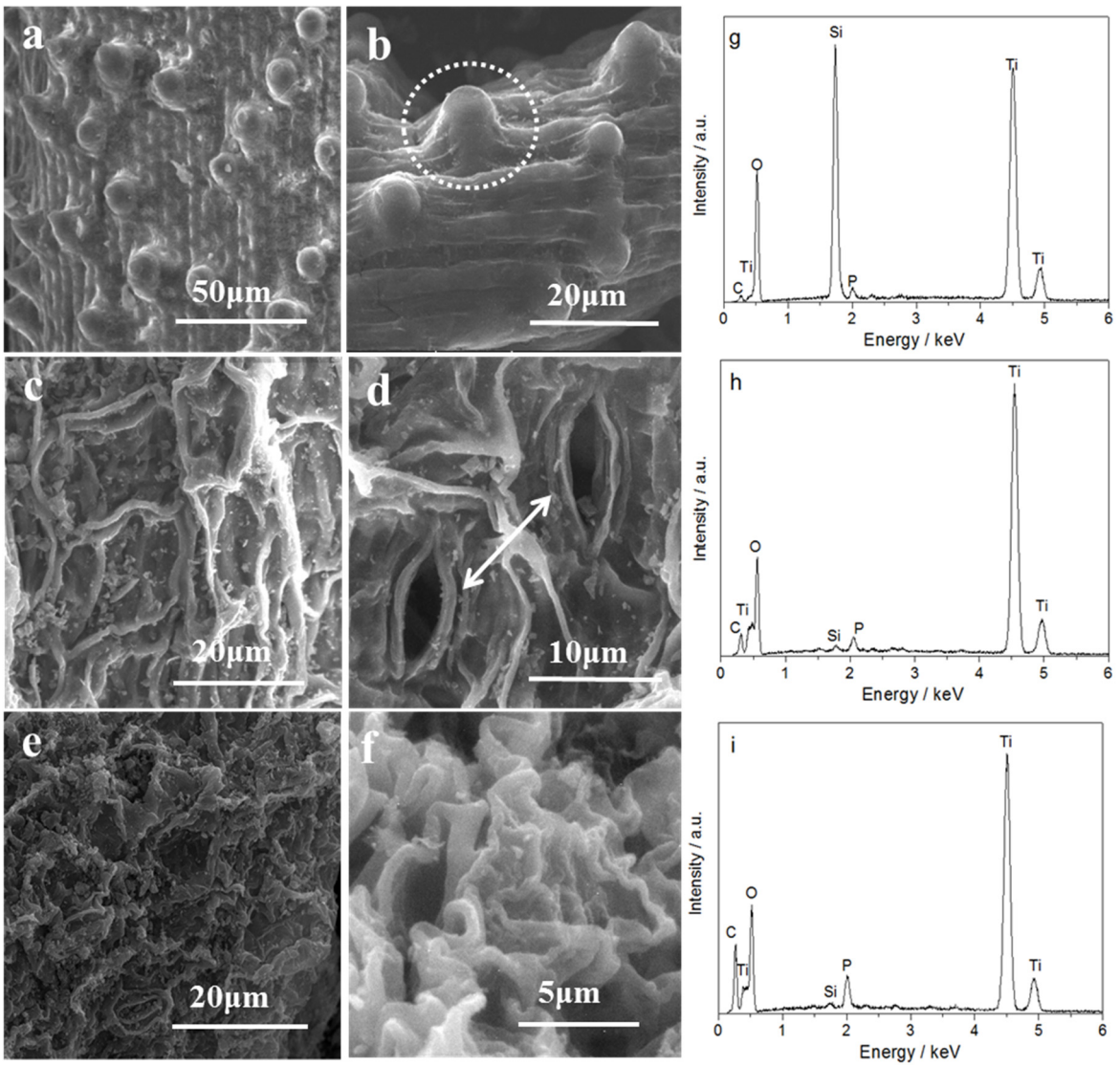

Figure 4. Scanning electron microscopy (SEM) images and energy dispersive X-ray spectroscopy (EDS) spectra: (**a**) original reeds; (**b**) and (**g**) R-TiO_2/SiO_2; (**c**) original water hyacinth; (**d**) and (**h**) WH-TiO_2/SiO_2; (**e**) original duckweed; (**f**) and (**i**) D-TiO_2/SiO_2.

Figure 5a–c show the Transmission electron microscopy (TEM) images of the biotemplated TiO_2/SiO_2 derived from reed, water hyacinth, and duckweed leaves. It was found that all biotemplated TiO_2/SiO_2 frameworks display the honeycomb mesoporous structure composed of fine particulate, which is consistent with results obtained by N_2 adsorption/desorption measurements. In particular, in Figure 5a, the linear and parallel skeleton of veins originating from reed leaf can be observed in R-TiO_2/SiO_2 frameworks.

The corresponding High-resolution TEM (HRTEM) images of the TiO_2/SiO_2 samples are displayed in Figure 5d–f, respectively. It can be found in Figure 5d,e that both the R-TiO_2/SiO_2 and WH-TiO_2/SiO_2 nanoparticles are of high crystallinity and good particle dispersion. On the contrary, D-TiO_2/SiO_2 nanoparticles, shown in Figure 5f, exhibit lower crystallinity, and are surrounded by an obvious organic carbon layer. Also, the average crystallite sizes, estimated from Figure 5d–f, are about 4, 8, and 4 nm for R-TiO_2/SiO_2, WH-TiO_2/SiO_2, and D-TiO_2/SiO_2, which is consistent with the result from by XRD analysis. Moreover, the lattice fringes of 3.50 Å shown in Figure 5g correspond to the (101) lattice planes of anatase TiO_2.

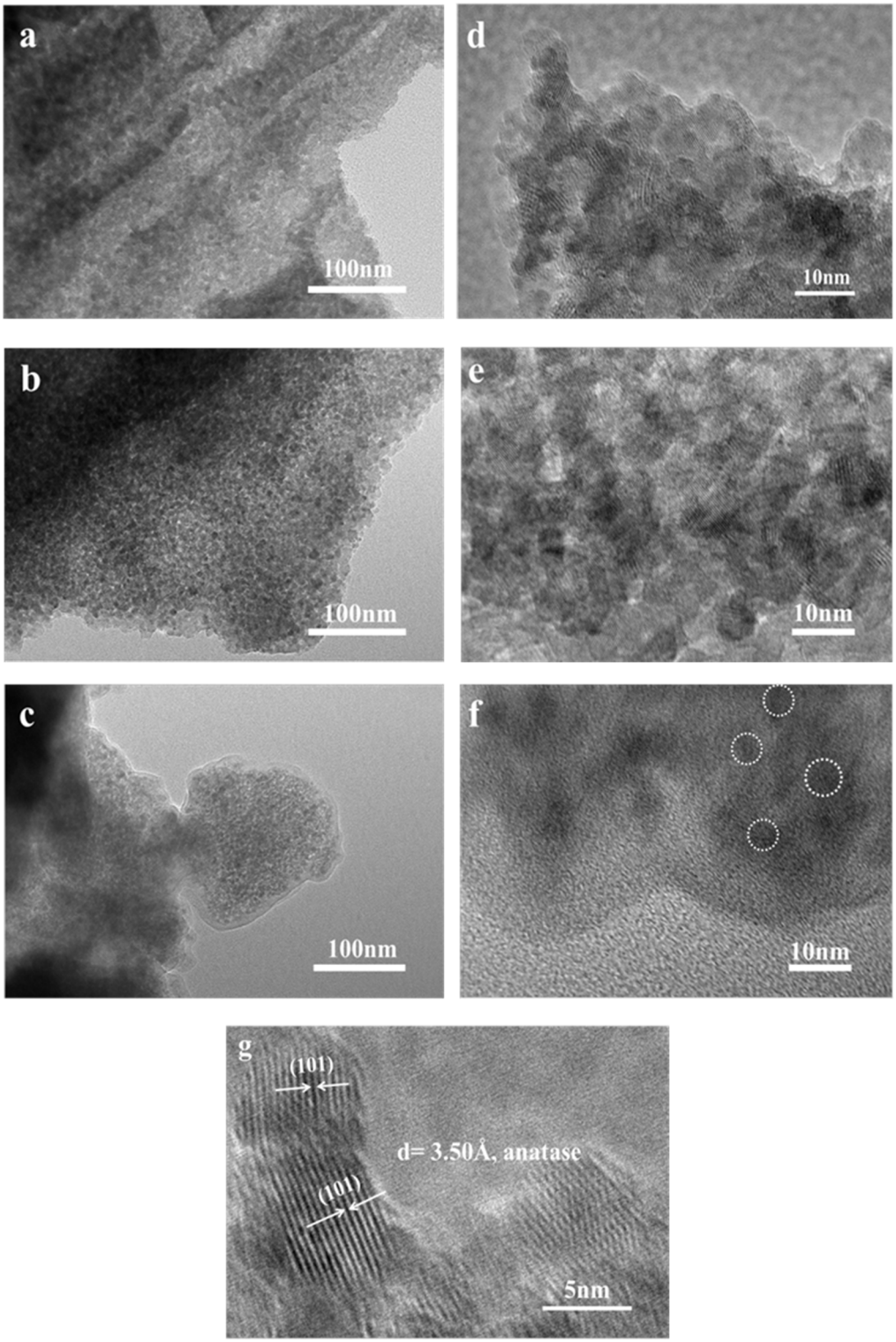

Figure 5. Transmission electron microscopy (TEM) and High-resolution TEM (HRTEM) images of (**a**), (**d**), and (**g**) R-TiO_2/SiO_2; (**b**) and (**e**) WH-TiO_2/SiO_2; (**c**) and (**f**) D-TiO_2/SiO_2.

2.2. Studies on Light-Harvesting and Photocatalytic Activities of TiO_2/SiO_2 Photocatalysts

UV–vis diffuse reflectance spectra of the TiO_2/SiO_2 samples along with P25 TiO_2 are shown in Figure 6. Compared with P25, the TiO_2/SiO_2 composites show significant enhancement in the visible-light areas. As everyone knows, neither pure SiO_2 nor bare TiO_2 exhibit visible-light absorption. All enhancements can be attributed to the biomorphic structure, which means "structure-introduced enhancement", as reported by Li [11] and Ma [15]. Briefly, the method here

realizes not only structure replication but also introduction of elements from biotemplates to TiO_2/SiO_2 samples, and thus the resultant TiO_2/SiO_2 composites inherit the enhanced visible-light-harvesting of plants. More notably, the blue shifts, as revealed in Figure 6, imply an increase in band gap energy of TiO_2/SiO_2 samples, which is similar to TiO_2–SiO_2 composites reported by Ma et al. [15]. The corresponding band gap energies estimated by Equation (1) are shown in Table 2, where E_g is the band gap energy (eV), and λ is the wavelength of adsorption edge (nm).

$$E_g = 1240/\lambda \quad (1)$$

It can be seen that the band gap energies are about 3.25, 3.22, and 3.21 eV for R-TiO_2/SiO_2, WH-TiO_2/SiO_2, and D-TiO_2/SiO_2 samples, respectively, which are higher than that of P25 (3.16 eV) and pure anatase (3.2 eV). As known, P25 TiO_2 is composed of both rutile and anatase TiO_2, whereas the TiO_2/SiO_2 samples from aquatic plants are almost in pure anatase phase based on the XRD spectra. It is well known that band gap energy of pure anatase is higher than bulk rutile TiO_2, and thus the unique anatase content of the biotemplated samples result in a raise in band gap energy [15]. Besides, Jafry et al. [7] and Malinowska et al. [25] presented that the change in the band gap energy of TiO_2–SiO_2 composites, prepared by an in situ doping of SiO_2, results from the reduction of valence band and the increase of conduction band. In this work, the band gap energy seems to be increasing slowly with the change in Si content, which will help to improve the efficiency of electron–hole separation, thus leading to efficient photocatalysis. In short, no extra silicon source is used in our method, and the visible-light-harvesting properties of biotemplate TiO_2/SiO_2 composites were enhanced.

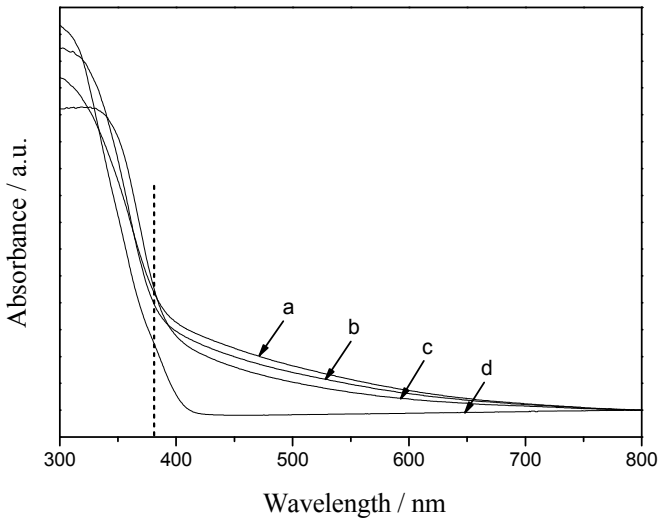

Figure 6. UV–vis diffuse reflectance spectra of (a) R-TiO_2/SiO_2; (b) WH-TiO_2/SiO_2; (c) D-TiO_2/SiO_2; and (d) P25.

Table 2. Band gap energy calculated by UV–vis diffuse reflectance spectra.

Samples	E_g (eV)
P25	3.16
R-TiO_2/SiO_2	3.25
WH-TiO_2/SiO_2	3.22
D-TiO_2/SiO_2	3.21

Photocatalytic activities were studied by degrading gentian violet (GV) dye in the presence of TiO_2/SiO_2 samples, P25, and TiO_2-p (TiO_2 particles prepared without template) under simulated sunlight irradiation. To achieve real photocatalytic degradation owing to photocatalysis in the presence of photocatalysts, the adsorption yield of dye was investigated. When adsorption–desorption equilibrium was reached after 12 h in the dark, the adsorption yields (shown in Table 3)

are 62.4%, 51.5%, and 43% for R-TiO_2/SiO_2, WH-TiO_2/SiO_2, and D-TiO_2/SiO_2 samples, respectively, which is much higher than 7.4% for P25 and 20.6% for TiO_2-p. The strong adsorption effect is relative to their higher specific surface area, as reported by Anderson et al. [6].

Table 3. Adsorption and degradation yields of gentian violet (GV) over the biotemplated samples and P25.

Samples	Adsorption Yields (%)	Degradation Yields (%)
R-TiO_2/SiO_2	62.4	72.0
WH-TiO_2/SiO_2	51.5	61.4
D-TiO_2/SiO_2	43.0	11.7
P25	7.4	42.4
TiO_2-p	20.6	24.5

After deducting the decreases of dye concentration due to adsorption and direct photolysis, the real photocatalytic degradation owing to the photocatalysis in the presence of photocatalysts was obtained and is shown in Figure 7. The degradation yields of biotemplated samples after 5 h are 72.0%, 61.4%, and 11.7% for the R-TiO_2/SiO_2, WH-TiO_2/SiO_2, and D-TiO_2/SiO_2 composites. In particular, R-TiO_2/SiO_2 and WH-TiO_2/SiO_2 samples possess better photocatalytic activities than P25 TiO_2 and TiO_2-p. For the D-TiO_2/SiO_2 sample, the degradation yield increases to 15.6% in 3 h, then slowly decreases to 11.7% in 5 h, which is lower than P25 TiO_2 and TiO_2-p. The results indicate that biotemplating may play an important role in improving photocatalytic activity, and that the activity is closely related to the plant species used as templates to duplicate photocatalysts.

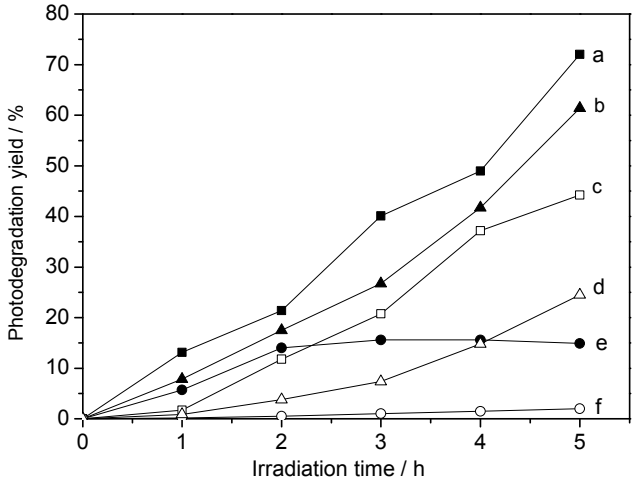

Figure 7. Photocatalytic degradation curves of GV, under solar light irradiation, for (a) R-TiO_2/SiO_2; (b) WH-TiO_2/SiO_2; (c) P25; (d) TiO_2-p; (e) D-TiO_2/SiO_2; and (f) no catalysts.

According to the experimental results, it can be deduced that the SiO_2 incorporation and structural construction should be the primary factors devoted to photocatalytic performance enhancement. On the one hand, it should be noted that the introduction of Si has been reported to improve not only the specific surface area but also the visible-light-harvesting of TiO_2/SiO_2 [14,15]. In this work, with Si introduced, the TiO_2/SiO_2 samples, particularly R-TiO_2/SiO_2 composites, show a large specific surface area and enhanced visible-light harvesting. Additionally, the photocatalytic activities were improved successively with Si content in the order of D-TiO_2/SiO_2, WH-TiO_2/SiO_2, and R-TiO_2/SiO_2 composites. On the other hand, as described above, the unique structural features derived from the natural plant leaves endow them with a great light-adsorbing capability. In particular, the papillae and stomatas in leaves were duplicated, respectively, to R-TiO_2/SiO_2 and WH-TiO_2/SiO_2 samples. Such structures are favorable for light harvesting [11,15]. Also, the highly crystalline mesoporous structure in R-TiO_2/SiO_2 and WH-TiO_2/SiO_2 catalysts, which also originated from the natural hierarchical structures of the plant templates, endowed them larger specific

surface areas, and more adsorption and active sites, which are conducive to quickening mass transport and improving the efficiency of electron–hole separation [26]. Besides, the increasing band gaps in TiO_2/SiO_2 samples as a result of the structure and introduction of Si could reduce electron–hole recombination, and help to capture more photoinduced holes during the photocatalytic process [26,27]. Therefore, in this work, the photocatalytic activity of R-TiO_2/SiO_2 and WH-TiO_2/SiO_2 samples was higher than that of P25 TiO_2 and TiO_2-p. In the case of D-TiO_2/SiO_2 samples, although it possesses high specific surface area and band gaps, the negligible Si content appears to dampen the effect on its photocatalytic activity. In particular, the presence of a large amount of organic carbon led to its lower crystalline structure, which is not conducive to improving the photocatalytic activity. Besides, lack of special structural characteristics for original duckweed may also be a factor that leads to the poorer photocatalytic activity compared to R-TiO_2/SiO_2 and WH-TiO_2/SiO_2. As a result, a synergistic effect of SiO_2 incorporation and structural construction through biotemplating is suggested to be beneficial to photocatalytic activity.

3. Materials and Methods

3.1. Synthesis

TiO_2 samples were synthesized by using a sol–gel process according to our previous works [28]. Firstly, fresh leaves were carefully rinsed with deionized water several times to remove the plankton and other impurities adsorbed on the surface. Then, the leaves were cut into little pieces and soaked in 2% glutaraldehyde/phosphate-buffered saline (PBS; pH = 7.2) solution at 4 °C for 12 h to fix the structures of plants. Secondly, the fixed leaves were immersed in HCl solution of 5% for 3 h until the green leaves became yellow-green, then, immersed in 5% $TiCl_3$ solution for 1 day. The as-treated leaves were gradually dehydrated in ethanol (30%, 60%, 90%, and 100%, respectively) and then were treated by sol infiltration of TTIP/ethanol/ACAC solution (volume ratio of 1:29:0.1) for 3 days. After filtration and washing with ethanol several times to remove any superfluous titanium source completely, the infiltrated samples were hydrolyzed in air for 4 days. Finally, the hydrolyzed samples were dried at 90 °C for 12 h, calcined at 280 °C for 2 h and at 450 °C for 6 h to remove the biotemplates and crystallize the TiO_2. Finally, the, grey-white products were formed. The samples templated by reed leaves, water hyacinth and duckweed are designated as R-TiO_2/SiO_2, WH-TiO_2/SiO_2, and D-TiO_2/SiO_2, respectively. For comparison, the TiO_2-p particles were prepared by the same sol–gel method in the absence of any template.

3.2. Characterizations

Powder X-ray diffraction (XRD) was performed on a TTR III spectrometer with Cu Kα radiation (Rigaku D/max-3B, Tokyo, Japan). Scanning electron microscopy (SEM) images of the samples were taken on a FEIQuanta 200FEG microscope (FEI, Eindhoven, Netherlands) with energy dispersive X-ray spectroscopy (EDS, Oxford INCA, Abingdon, Oxfordshire, UK) at 5 kV. X-ray fluorescence (XRF) analysis was measured on a ZSX100E spectrometer (Rigaku, Tokyo, Japan). Pore size distributions, BET surface areas, and BJH pore size distribution were determined by nitrogen adsorption–desorption using a Tristar II 3020 surface area and porosity analyzer (Micromeritics, Norcross, GA, USA). Fourier-transform infrared spectrum (FTIR) measurement was conducted on a Thermo Nicolet AVATAR FT-IR 360 instrument (Thermo Nicolet Corp., Madison, WI, USA). UV–vis diffuse reflectance spectra were measured on a UV-2401PC photometer (Shimadzu, Kyoto, Japan).

3.3. Catalytic Performance

Photocatalytic degradation of GV ($C_{25}H_{30}ClN_3$) was performed on an XPA-7 photochemical reactor (Xujiang Electromechanical Plant, Nanjing, China). Suspended solutions containing 50 mL of 10 mg/L GV solution and 20 mg photocatalyst were stirred in the dark for 12 h to achieve adsorption–desorption equilibrium between dyes and TiO_2 photocatalysts. After that, the reactor was illuminated under simulated sunlight irradiation through an 800 W xenon lamp. Samples were

tested after centrifugation for 10 min. The change of the dye concentration was measured by Shimadzu UV-2401PC photometer in the range of 400–800 nm.

In order to investigate the real photocatalytic degradation owing to the photocatalysis in the presence of photocatalysts, the decreases of dye concentration caused by adsorption and self-degradation should be deducted. Therefore, the adsorption yield and photodegradation yield were separately calculated by the following Equations (2) and (3) [28]:

$$\text{adsorption yield (\%)} = (C - C_0) \times 100\%/C \quad (2)$$

$$\text{photodegradation yield (\%)} = (C_0 - C_a - C_b) \times 100\%/C_0 \quad (3)$$

where C is the initial concentration before adsorption, C_0 is the concentration after adsorption–desorption equilibrium between dyes and TiO_2 photocatalysts before light irradiation, C_a is the concentration after photodegradation under simulated solar light, and C_b is the decrease in dye concentration because of the direct photolysis in the presence of no catalyst. For C_b, it equals ($C - C_a$).

The activity of Degussa P25 TiO_2 and TiO_2-p particles was also measured under the same conditions.

4. Conclusions

A simple biotemplated method was provided to successfully synthesize TiO_2/SiO_2 composites without using any extra Si precursors or chemical templates. The resulting TiO_2/SiO_2 composites may simultaneously attain the duplication of structure and self-doping Si from aquatic plant leaves including reed, water hyacinth, and duckweed. All TiO_2/SiO_2 composites display a high specific surface area and intensive light-harvesting efficiency, particularly in the visible light range. The TiO_2/SiO_2 samples templated by reed and water hyacinth leaves exhibit efficient activity for the photodegradation of gentian violet under simulated solar irradiation, while the TiO_2/SiO_2 sample obtained from duckweed was inferior to P25 and TiO_2-p without any template. The SiO_2 incorporation and structural duplication should be the primary factors considered for the contribution to the photocatalytic activity. Also, the activity is closely related to the plant species used as templates to duplicate photocatalysts. The resulting TiO_2/SiO_2 composites could be applied as photocatalysts and adsorbing materials for degradation and removal of harmful substances.

Supplementary Materials: The following are available online at www.mdpi.com/2073-4344/7/3/82/s1, Figure S1: Nitrogen adsorption–desorption isotherms of (a) WH-TiO_2/SiO_2 and (b) D-TiO_2/SiO_2 samples; BJH pore size distributions of (c) WH-TiO_2/SiO_2 and (d) D-TiO_2/SiO_2 sample.

Acknowledgments: The authors thank the National Natural Science Foundation of China (Project 21367024, 21263027, 21403190 and 21573193), Yunnan Applied Basic Research Projects (Project 2016FA002), the Program for Innovative Research Teams (in Science and Technology) in the University of Yunnan Province (IRTSTYN), Key Laboratory of Wastewater Treatment Materials of Kunming and the Key project from the Yunnan Educational Committee (Project ZD2012003) for financial support.

Author Contributions: Zhiying Yan, Jiaqiang Wang conceived and designed the experiments; Yueting Li, Fagui Yuan performed the experiments; Deliang Duan, Junjie Li and Yongjuan Chen analyzed the data; Zhiying Yan and Jiao He wrote the paper; Lei Guo revised the paper.

Conflicts of Interest: The authors declare no conflict of interest.

References

1. Kubacka, A.; Fernandez-Garcia, M. Advanced nanoarchitectures for solar photocatalytic applications. *Chem. Rev.* **2012**, *112*, 155–1614.
2. Liu, L.; Liu, H.; Zhao, Y. Directed synthesis of hierarchical nanostructured TiO_2 catalysts and their morphology-dependent photocatalysis for phenol degradation. *Environ. Sci. Technol.* **2008**, *42*, 2342–2348.
3. Yu, J.G.; Su, Y.R.; Cheng, B. Template-free fabrication and enhanced photocatalytic activity of hierarchical macro-/mesoporous titania. *Adv. Funct. Mater.* **2007**, *62*, 35–50.
4. Todorova, N.; Vaimakis, T.; Petrakis, D.; Hishita, S.; Boukos. N. N and N, S-doped TiO_2 photocatalysts and their activity in NO_x oxidation. *Catal. Today* **2013**, *209*, 41–46.

5. Fu, X.; Clark, L.A.; Yang, Q.; Anderson, M.A. Enhanced photocatalytic performance of titania-based binary metal oxides: TiO_2/SiO_2 and TiO_2/ZrO_2. *Environ. Sci. Technol*. **1996**, *30*, 647–653.
6. Anderson, C.; Bard, A.J. Improved photocatalytic activity and characterization of mixed TiO_2/SiO_2 and TiO_2/Al_2O_3 materials. *J. Phys. Chem*. **1997**, *101*, 2611–2616.
7. Jafry, H.R.; Liga, M.V.; Li, Q.; Barron, A.R. Simple route to enhanced photocatalytic activity of P25 titanium dioxide nanoparticles by silica addition. *Environ. Sci. Technol*. **2011**, *45*, 1563–1568.
8. Jafry, H.R.; Liga, M.V.; Li, Q.; Barron, A.R. Single walled carbon nanotubes (SWNTs) as templates for the growth of TiO_2: The effect of silicon in coverage and the positive and negative synergies for the photocatalytic degradation of Congo red dye. *New J. Chem*. **2011**, *35*, 400–406.
9. Zhang, C.; Mcadams, D.A., II; Grunlan, J.C. Nano/micro-manufacturing of bioinspired materials: A review of methods to mimic natural structures. *Adv. Mater.* **2016**, *28*, 6292–6321.
10. Han, T.; Fan, T.X.; Chow, S.K.; Zhang D. Biogenic N-P-codoped TiO_2: Synthesis, characterization and photocatalytic properties. *Bioresour. Technol.* **2010**, *101*, 6829–6835.
11. Li, X.; Fan, T.; Zhou, H.; Chow, S.K.; Zhang, W.; Zhang, D.; Guo, Q.; Ogawa, H. Enhanced light-harvesting and photocatalytic properties in morph-TiO_2 from green-leaf biotemplates. *Adv. Funct. Mater.* **2009**, *19*, 45–56.
12. Dorian, A.H.H.; Sorrell, C.C. Sand supported mixed-phase TiO_2 photocatalysts for water decontamination applications. *Adv. Eng. Mater.* **2014**, *16*, 248–254.
13. Kibombo, H.S.; Zhao, D.; Gonshorowski, A.; Budhi, S.; Koppang, M.D.; Koodali, R.T. Cosolvent-induced gelation and the hydrothermal enhancement of the crystallinity of titania-silica mixed oxides for the photocatalytic remediation of organic pollutants. *J. Phys. Chem. C* **2011**, *115*, 6126–6135.
14. Yang, D.L.; Fan, T.X.; Zhou, H.; Ding, J.; Zhang, D. Biogenic hierarchical TiO_2/SiO_2 derived from rice husk and enhanced photocatalytic properties for dye degradation. *PLoS ONE* **2011**, doi:10.1371/journal.pone.0024788.
15. Ma, H.; Liu, W.W.; Zhu, S.W.; Ma, Q.; Fan, Y.S.; Cheng, B.J. Biotemplated hierarchical TiO_2-SiO_2 composites derived from *Zea mays* Linn. for efficient dye photodegradation. *J. Porous Mater.* **2013**, *20*, 1205–1215.
16. Liu, J.; Yang, Q.; Yang, W.; Li, M.; Song, Y. Aquatic plant inspired hierarchical artificial leaves for highly efficient photocatalysis. *J. Mater. Chem.* **2013**, *1*, 7760–7766.
17. Okada, K.; Yamamoto, N.; Kameshima, Y.; Yasumori, A.; Mackenzie, K.J.D. Effect of silica additive on the anatase-to-rutile phase transition. *J. Am. Ceram. Soc.* **2004**, *84*, 1591–1596.
18. Dirken, P.J.; Smith, M.E.; Whitfield, H.J. ^{17}O and ^{29}Si solid state NMR study of atomic scale structure in sol-gel-prepared TiO_2-SiO_2 materials. *J. Phys. Chem.* **1995**, *99*, 395–401.
19. Ren, J.; Li, Z.; Liu, S.; Xing, Y.; Xie, K. Silica-titania mixed oxides: Si–O–Ti connectivity, coordination of titanium, and surface acidic properties. *Catal. Lett.* **2008**, *124*, 185–194.
20. Li, Y.Z.; Kim, S.J. Synthesis and characterization of nano titania particles embedded in mesoporous silica with both high photocatalytic activity and adsorption capability. *J. Phys. Chem. B* **2005**, *109*, 12309–12315.
21. Leofanti, G.; Padovan, M.; Tozzola, G.; Venturelli, B. Surface area and pore texture of catalysts. *Catal. Today* **1998**, *41*, 207–219.
22. Yu, X.X.; Yu, J.G.; Cheng, B.; Jaroniec, M. Synthesis of hierarchical flower-like AlOOH and TiO_2/AlOOH superstructures and their enhanced photocatalytic properties. *J. Phys. Chem. C* **2009**, *113*, 17527–17535.
23. Poulson, M.E.; Vogelmann, T.C. Epidermal focussing and effects upon photosynthetic light-harvesting in leaves of *Oxalis*. *Plant Cell Environ.* **1990**, *13*, 803–811.
24. Zhou, H.; Li, X.; Fan, T.; Osterloh, F.E.; Ding, J.; Sabio, E.M.; Zhang, D.; Guo, Q. Artificial inorganic leafs for efficient photochemical hydrogen production inspired by natural photosynthesis. *Adv. Mater.* **2010**, *22*, 951–956.
25. Malinowska, B.; Walendziewski, J.; Robert, D.; Weber, J.V.; Stolarski, M. The study of photocatalytic activities of titania and titania silica aerogels. *Appl. Catal. B* **2003**, *46*, 441–451.
26. Chen, X.F.; Wang, X.C.; Fu, X.Z. Hierarchical macro/mesoporous TiO_2/SiO_2 and TiO_2/ZrO_2 nanocomposites for environmental photocatalysis. *Energy Environ. Sci.* **2009**, *2*, 872–877.
27. Dong, W.Y.; Lee, C.W.; Lu, X.C.; Sun, Y.J.; Hua, W.M.; Zhuang, G.S.; Zhang, S.C.; Chen, J.M.; Hou, H.Q.; Zhao, D.Y. Synchronous role of coupled adsorption and photocatalytic oxidation on ordered mesoporous anatase TiO_2-SiO_2 nanocomposites generating excellent degradation activity of RhB dye. *Appl. Catal. B* **2009**, *95*, 197–207.

28. Tao, J.; Gong, W.; Yan, Z.; Duan, D.; Zeng, Y.; Wang, J. UV/visible-light photodegradation for organic dyes over mesoporous titania prepared by using 2,4,5-triphenylimidazole as template. *Mater. Sci. Semicond. Process.* **2014**, *27*, 452–460.